RSC Advances

PAPER

View Article Online
View Journal | View Issue

Cite this: *RSC Adv.*, 2026, **16**, 12295

Unusual prenylated phenols with antioxidant and immunosuppressive activities from the edible mushroom *Lentinula edodes*

Zhen-Zhu Zhao, † Fei Zhang,†* Qi-Lu Zhao, Jie Zhao, Hai-Rong He, Hai-Jiao Liu, Ke-Ke Liu and Hui Chen *

Received 18th December 2025
Accepted 25th February 2026

DOI: 10.1039/d5ra09796g

rsc.li/rsc-advances

Prenylated phenols, the primary class of mushroom-derived meroterpenoids, exhibit significant structural diversity and biological activities. Two new prenylated phenols (**1** and **2**), along with four aromatic derivatives, were isolated from the wild mushroom *Lentinula edodes* for the first time. Their structures were established based on extensive spectroscopic data (UV, IR, MS, and NMR) and further corroborated by X-ray crystallographic analysis. Compounds **1** and **2** are unusual meroterpenoids characterized by 4-prenylated benzene 1,2,3-triols or 3-prenylated benzene 1,2-diols. Compound **2** showed moderate immunosuppressive activity by inhibiting the proliferation of induced T/B cells; it also demonstrated inhibitory effects on the proliferation of the HaCaT cell line (IC_{50} 24.5 μM) and antioxidant activity at 50 μM.

Introduction

Meroterpenoids are hybrid natural products partly derived from the terpenoid biosynthetic pathway.[1] These compounds are distinguished by their unique and complex carbon skeletons, as well as diverse bioactivities, including anticancer effects, BACE1 inhibition, anti-inflammatory properties, and lipid-lowering abilities.[2–4] Due to their structural distinctiveness and pharmacological potential, meroterpenoids have attracted significant attention from chemists and pharmacologists. These specialized metabolites are produced by various organisms, including plants, animals, bacteria, and fungi, with fungi being among the most prolific sources, capable of biosynthesizing a wide range of meroterpenoid derivatives. In 2009 and 2021, Geris and Zhao published comprehensive reviews on fungal-derived meroterpenoids (covering both higher and lower fungi), systematically exploring their structural diversity and biological activities. Notably, species from the genera *Ganoderma*, *Penicillium*, and *Aspergillus* are the primary producers, responsible for over 50% of all reported meroterpenoids.[2,3] In mushrooms, most meroterpenoids are prenylated phenol derivatives. To date, mushroom-derived meroterpenoids have been mainly isolated from *Ganoderma*, *Suillus*, *Albatrellus*, and *Russula* species, with over 90% of the prenylated phenol derivatives originating from *Ganoderma* alone.[2,3,5]

Most mushroom-derived meroterpenoids are 2-prenylated benzene 1,4-diols (A-type), especially suitable for those from *Ganoderma*; several are 2-prenylated benzene 1,3-diols (B-type) or 3-prenylated benzene 1,2,4-triols (C-type) (Fig. 1).[2,3,6,7] To the best of our knowledge, 3-prenylated benzene-1,2-diols (D-type) remain unreported.

Edible mushrooms are widely recognized as health-promoting foods due to their unique nutritional profiles, characterized by low caloric content and a rich supply of essential nutrients, including vitamins and minerals. Among these, *Lentinula edodes* (shiitake mushroom) is a prominent species valued for both its culinary and medicinal properties, with a long history of consumption in East Asia.[8,9] In our previous investigation, we identified a series of pyrrole-containing alkaloids from the wild *L. edodes* fruiting bodies.[10] Continuing our research on this species, we have now isolated two novel prenylated phenolic metabolites.

In this study, we report the isolation and structural elucidation of six compounds (**1–6**, Fig. 2). Notably, compounds lentinuines A (**1**) and B (**2**) are unusual meroterpenoids characterized by a 4-prenylated benzene 1,2,3-triols (**1**) or 3-prenylated benzene 1,2-diols (**2**) (D-type). Additionally, we assessed their potential bioactivities, including cytotoxicity against a keratinocyte cell line and T/B lymphocytes, as well as their free radical scavenging ability using the 2,2-diphenyl-1-picrylhydrazyl (DPPH) assay.

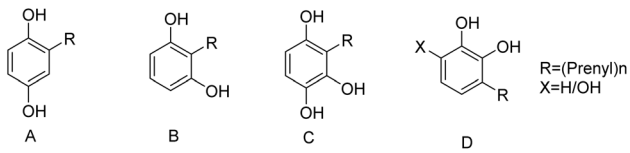

Fig. 1 Substitution pattern of aromatic rings in meroterpenoids.

School of Pharmacy, Henan University of Chinese Medicine, Zhengzhou 450046, China. E-mail: chenhuiyxy@hactcm.edu.cn; zhfei0123@163.com

† These authors contributed equally to this work.

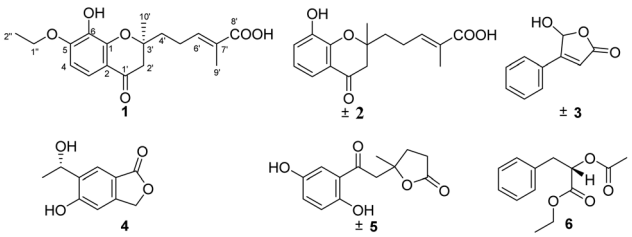

Fig. 2 Structures of compounds 1–6.

Results and discussion

Compound **1** was isolated as a yellow oil. HRESIMS analysis determined the molecular formula as $C_{18}H_{22}O_6$ (8 degrees of unsaturation), based on the ion at *m*/*z* 357.1313 $[M + Na]^+$ (calc. 357.1309 for $C_{18}H_{22}O_6Na^+$). The UV spectrum exhibited absorption maxima at 211, 273, and 361 nm, while the IR spectrum indicated the presence of two conjugated carbonyl (1683 and 1607 cm^{-1}) functionalities. The ^1H NMR spectrum (Table 1) displayed signals corresponding to three aromatic/olefinic hydrogens [δ_H 6.99 (d, J = 8.9 Hz); 6.74 (t, J = 7.0 Hz); 6.44 (d, J = 8.9 Hz)], three methyl groups [δ_H 1.77 (s), 1.45 (s), 1.38 (t, J = 7.0 Hz)], and eight methylene/methine protons [δ_H 4.01 (q, J = 7.0 Hz, 2H); 2.81 (d, J = 15.8 Hz); 2.70 (d, J = 15.8 Hz); 2.36 (m, 2H); 1.90 (m), 1.82 (m)]. The ^{13}C NMR and DEPT spectra (Table 1) resolved seventeen carbon resonances, classified as three methyl carbons (δ_C 24.0, 15.0, 12.3), four methylene carbons (including one oxygenated carbon at δ_C 66.1), three aromatic/olefinic methine carbons (δ_C 142.6, 123.0, 105.9), one sp^3 oxygenated quaternary carbon (δ_C 82.0), five olefinic quaternary carbons (δ_C 153.3, 150.0, 141.2, 129.6, 112.5), and a conjugated ketone (δ_C 193.8). A conjugated carboxyl group was identified (δ_C 171.8), whose signal, although weak, remained detectable in the 1D NMR spectrum. Its assignment was ultimately confirmed by key correlations observed in the HMBC spectrum. Analysis of the 1D NMR data suggested a bicyclic system to account for the remaining two degrees of unsaturation. HSQC correlations assigned all proton resonances to their respective carbons. The planar structure of **1** was deduced to consist of two rings and a side chain, supported by the following key observations: AB-coupled aromatic system [$\delta_{C/H}$ 123.0/6.99 (d, J = 8.8 Hz); 105.9/6.44 (d, J = 8.8 Hz)], an α,β-unsaturated carboxyl group [$\delta_{C/H}$ 142.6/6.74 (t, J = 7.4 Hz), 171.7, 12.3/1.77(s)], and an ethoxy group [$\delta_{C/H}$ 66.1/4.01 (q, J = 7.0 Hz), 15.0/1.38 (t, J = 7.0 Hz)]. HMBC correlations further confirmed the connectivity: H-1″ → C-2″/C-5, H-4 → C-6, and H-3 → C-1/C-2/C-5/C1′ (Fig. 3). These data established a 1,6-dihydroxy-5-ethoxy-4-(1′-one) aromatic ring. Additionally, HMBC correlations from CH_3-10′ → C-2′/C-3′/C-4′, H_2-2′ → C-1′, and CH_3-9′ → C-6′/C-7′/C-8′, H_2-6′ → C-5′ revealed two isopentyl groups: a 3′-hydroxy-1′-one-isopentyl group (C1′-C4′, C10′) and an isopenoic acid group (C5′–C9′). These fragments were connected to form a 3′-hydroxy-1′-oxo-monoterp-6′-en-8′-oic acid (C1′–C10′), supported by HMBC correlations from H-6′/H_2-5′ → H-4′. This monoterpenoid unit was linked to the 1,6-dihydroxy-5-ethoxy-4-benzene moiety *via* C1–C1′, as evidenced by HMBC correlations from H_2-2′ → C-1 and H-3 → C-1′. The remaining degree of

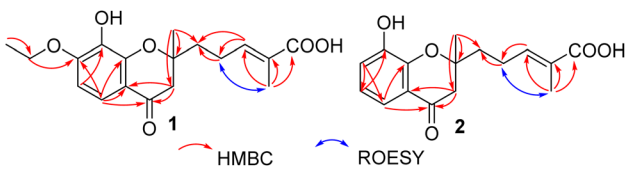

Fig. 3 Key 2D NMR correlation of **1** and **2**.

Table 1 ^{13}C (150 MHz) and ^1H (600 MHz) NMR data of **1** and **2** (δ in ppm)

	1[a]		1[b]	2[a]	
No.	δ_C	δ_H (J in Hz)		δ_C	δ_H (J in Hz)
1	141.2, C	—	140.4	149.6, C	—
2	112.5, C	—	111.3	122.3, C	—
3	105.9, CH	6.44, d (8.9)	104.7	117.4, CH	7.29, dd (8.0, 1.6)
4	123.0, CH	6.99, d (8.9)	121.2	121.7, CH	6.84, dd (8.0, 8.0)
5	153.3, C	—	151.1	122.6, CH	7.06, dd (8.0, 1.6)
6	150.0, C	—	148.4	148.1, C	—
1′	193.8, C	—	190.2	194.8, C	—
2′	49.7, CH_2	2.81, d (15.8); 2.70, d (15.8)	48.5	48.3, CH_2	2.85, d (16.7); 2.77, d (16.7)
3′	82.0, C	—	80.2	82.5, C	—
4′	38.2, CH_2	1.90, m; 1.82, m	37.0	38.2, CH_2	1.92, m; 1.83, m
5′	23.9, CH_2	2.36, m	22.4	24.0, CH_2	2.38, m
6′	142.6, CH	6.74, t (7.0)	140.1	142.5, CH	6.74, t (7.8)
7′	129.6, C	—	128.5	129.8, C	—
8′	171.7, C	—	169.2	171.8, C	—
9′	12.3, CH_3	1.77, s	12.2	12.3, CH_3	1.77, s
10′	24.0, CH_3	1.45, s	23.2	24.1, CH_3	1.48, s
1″	66.1, CH_2	4.01, q (7.0)	64.3		—
2″	15.0, CH_3	1.38, t (7.0)	14.7		—

[a] Measured in CD_3OD. [b] Measured in DMSO-d_6.

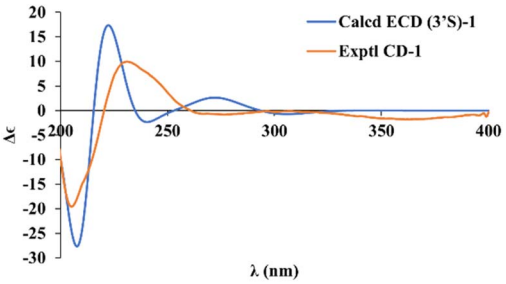

Fig. 4 A comparison between the experimental CD spectrum of **1** (in MeOH) and its simulated ECD spectrum (with parameters $\sigma = 0.3$ eV and UV shift of 5 nm).

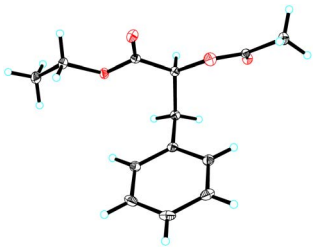

Fig. 5 ORTEP drawing of **6**.

unsaturation indicated a second ring, formed *via* dehydration-condensation between 1-OH and 3′-OH, consistent with the downfield shift of C-1 (δ_C 141.2) and upfield shift of C-3′ (δ_C 82.0). Thus, **1** was identified as a meroterpenoid with a chromone core. ROESY correlations between H_2-5′ and H_3-9′ suggested an *E*-configuration at $\Delta^{6'(7')}$. Since **1** contains only one chiral center (C-3′), two configurations were possible: (3′*R*)-**1** or (3′*S*)-**1**. Chiral HPLC confirmed optical purity (Fig. S19, SI), and ECD calculations matched the experimental spectrum for (3′*S*)-**1** (Fig. 4). Additionally, the calculated optical rotation ($[\alpha]_D$ + 74.4) agreed with experimental data ($[\alpha]_D^{25}$ + 26.3). Finally, the structure of **1** was unequivocally determined as (3′*S*,6′*E*)-5-(6-ethoxy-5-hydroxy-2-methyl-4-oxochroman-2-yl)-2-methylpent-2-enoic acid and named lentinuine A (Fig. 2).

Lentinuine B (**2**) was obtained as a yellow oil. HRESIMS established the molecular formula as $C_{16}H_{18}O_5$, which is 44 mass units (OCH_2CH_2) smaller than **1**, suggesting the absence of an ethoxy group. The UV spectrum of **2** exhibited absorption maxima at 213, 266, and 340 nm, consistent with the chromophore observed in **1**, indicating structural similarity. The ^{1}H and ^{13}C NMR spectra of **2** closely resembled those of **1** (Table 1), confirming their structural similarity. However, key differences were observed in the aromatic region. Compound **2** displayed an ABB′ coupling system [$\delta_{C/H}$ 117.4/7.29 (dd, J = 8.0, 1.6 Hz), 121.7/6.84 (dd, J = 8.0, 8.0 Hz), 122.6/7.06 (dd, J = 8.0, 1.6 Hz)], contrasting with an AB coupling system in **1** [$\delta_{C/H}$ 123.0/6.99 (d, J = 8.8 Hz); 105.9/6.44 (d, J = 8.8 Hz)]. The ethoxy group present in **1** [$\delta_{C/H}$ 66.1/4.01 (q, J = 7.0 Hz), 15.0/1.38 (t, J = 7.0 Hz)] was replaced by a proton in **2**, which was further supported by HMBC correlations. Based on HMBC analysis, the structure of **2** was determined to be 5-(8-hydroxy-2-methyl-4-oxochroman-2-yl)-2-methylpent-2-enoic acid (Fig. 3). ROESY correlations between H_2-5′ and H_3-9′ confirmed an *E* configuration for $\Delta^{6'(7')}$. Chiral HPLC analysis revealed two peaks of equal intensity (Fig. S20, SI), indicating that **2** is a racemic mixture. Therefore, (±) compounds **2** were identified (±) (6′*E*)-5-(8-hydroxy-2-methyl-4-oxochroman-2-yl)-2-methylpent-2-enoic acid.

By analysis and comparison of their NMR data with those documented in literature, the known compounds **3**–**6** were identified as 5-hydroxy-4-phenyl-2(5*H*)-furanone (**3**),[11] erinaceolactone B (**4**) ($[\alpha]_D^{25}$ − 30.7 (c 0.1, MeOH) calculated value −87.49),[12] orirubenone G (**5**),[13] and ethyl (α*S*)-α-(acetyloxy) benzenepropanoate (**6**) (Fig. 2).[14]

In the reference, since the absolute configurations of **4** and **6** were not determined, they were first determined using calculated methods and single X-ray diffraction data. By comparing the experimental optical rotation of erinaceolactone B (**4**) ($[\alpha]_D^{25}$ − 30.7 (*c* 0.1, MeOH)) with the calculated value of one possible configuration (*S*)-**4** ($[\alpha]_D$ − 87.5) (SI), it is implied that (*S*)-**4** is the suitable configuration. For compound **6**, single-crystal X-ray diffraction data showed that the configuration of the chiral carbon is *S* (Fig. 5).

Based on the structural analogy of compounds **1** and **2** to Trolox (a derivative of vitamin E) and the existence of a phenolic hydroxyl group, their DPPH radical-scavenging activity was assessed. Comparative analysis indicated that compound **2** possessed a higher radical-scavenging capacity than compound **1** (Table 2). It is well established that phenolic hydroxyl groups exhibit strong reducing capacity, as seen in antioxidant phenols. This property stems from the conjugation between the phenolic hydroxyl group and the aromatic ring, which facilitates proton release. In compound **1**, the phenolic hydroxyl hydrogen can form an intramolecular hydrogen bond with the oxygen of the adjacent ethoxy group. This stabilizing interaction consequently reduces its antioxidant activity relative to compound **2**.

Additionally, the structures of **1** and **2** resembled that of mycophenolic acid (MPA). MPA, a potent uncompetitive inhibitor of inosine monophosphate dehydrogenase (IMPDH), serves as an immunosuppressive agent by preventing excessive proliferation of T and B lymphocytes.[15,16] Furthermore, MPA has also demonstrated antitumor effects. As analogs of MPA, compounds **1** and **2** were tested for their ability to inhibit the proliferation of induced T and B lymphocytes and the HaCaT cell line. The bioassay results showed that both compounds **1** and **2** can inhibit the proliferation of induced T lymphocytes. However, only compound **2** also exhibited antiproliferative activity on induced B lymphocytes and HaCaT cells (Table 3).

Based on its superior antiproliferative activity, compound **2** was selected to investigate the molecular mechanisms involving

Table 2 DPPH free radical scavenging activity of **1** and **2**

Samples	*c* (μM)	Antioxidant rate (%)
Trolox	25	90.7 ± 0.1
1	50	3.3 ± 1.3
2	50	59.8 ± 0.6

Table 3 IC_{50} values of **1** and **2** against the proliferation of induced T (ConA), B lymphocytes (LPS) and HaCaT cells

Samples	IC_{50} (μM)		
	T	B	HaCaT
1	29.2 ± 2.4	>40	>40
2	23.2 ± 1.6	33.4 ± 1.9	24.5 ± 1.5
DEX	2.1 ± 0.3	0.9 ± 0.07	—
MTX	—	—	23.2 ± 1.8
MPA	0.04 ± 0.006	0.09 ± 0.01	—

IMPDH. Molecular docking analysis revealed that (*R*)-**2** interacts with IMPDH as follows (Fig. 6): (i) the hydrogen of the 6-OH group forms a hydrogen bond with GLN112, stabilizing the IMPDH–(*R*)-**2** complex; (ii) hydrophobic interactions occur between the 9′-CH_3 group and TYR110, the 10′-CH_3 group and ALA223, the 5′-CH_2 group and PHE139, and the aromatic ring and PHE139/ILE115. For (*S*)-**2** (Fig. 6): (i) the hydrogen of the 8′-COOH group contributes to stabilizing the IMPDH–(*S*)-**2** complex; (ii) hydrophobic interactions are observed between the 10′-CH_3/aromatic ring and ILE115, and between the 5′-CH_2/aromatic ring and PHE139. The calculated binding energies for (*R*)-**2** and (*S*)-**2** with IMPDH are −7.4 and −7.8 kcal mol^{-1}, respectively. Based on its structural similarity to mycophenolic acid (MPA) and molecular docking simulations indicating potential stable interactions with the IMPDH active site, these results suggest that compound **2** may exert its antiproliferative effects through IMPDH targeting.

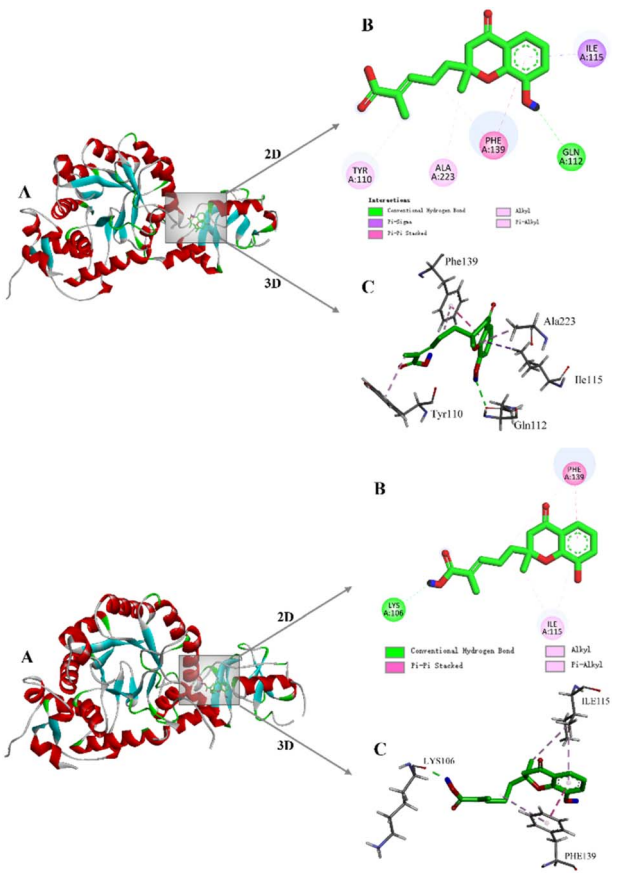

Fig. 6 Molecular docking analysis for predicted lowest-energy binding mode of IMPDH with (*R*)-**2** (top) and (*S*)-**2** (bottom), presented in both three-dimensional (A) and two-dimensional views (B and C) along with their corresponding binding affinities (−7.4 and −7.8 kcal mol^{-1}, respectively). In the ligand structure, carbon and oxygen atoms are highlighted in green and red, respectively. For the protein residues, the colors gray, red, and blue represent carbon, oxygen, and nitrogen atoms, respectively.

Conclusions

In summary, six aromatic derivatives were isolated from the wild edible mushroom *L. edodes*. Structurally, compounds **1** and **2** are unusual meroterpenoids featuring a 6-hydroxychroman-4-one scaffold, and were isolated for the first time from the fruiting bodies of this wild mushroom. While mushroom-derived meroterpenoids have been predominantly reported from genera such as *Ganoderma*, *Suillus*, *Albatrellus*, and *Russula*, the acquisition of **1** and **2** from wild *L. edodes* broadens the known origins of this class of metabolites. Biologically, both compounds, particularly **2**, demonstrated antioxidant and immunosuppressive activities. This study expands the known chemical constituents of wild *L. edodes* and enhances our understanding of this species.

Experimental section

General experimental procedures

Optical rotation values were recorded on a JASCO P-1020 digital polarimeter. UV spectra were obtained using a Shimadzu UV-2401PC recording spectrophotometer. IR spectra were acquired on a Thermo Scientific Nicolet iS10 FT-IR spectrometer. All NMR experiments were performed on a Bruker Avance III 600 MHz and 500 MHz spectrometers. HRESIMS data were generated using an Agilent 6200 Q-TOF mass spectrometer. Single-crystal X-ray diffraction intensity data were collected on a Bruker D8 Quest diffractometer. Melting points were determined with an X-4 microscopic melting point apparatus. Sephadex LH-20 (Amersham Biosciences, Uppsala, Sweden) and silica gel (Qingdao Haiyang Chemical Co., Ltd) were used for column chromatography (CC). For column chromatography, Sephadex LH-20 and silica gel were utilized. Medium-pressure liquid chromatography (MPLC) separations were achieved using either a Büchi Sepacore system (fitted with a Chromatorex C-18 column) or an FL-H050G MPLC system (equipped with an MCI gel column). Preparative HPLC (prep. HPLC) was performed on an Agilent 1260 system with DAD detection, employing Zorbax SB-C18 columns. Chiral-phase HPLC analysis was carried out on an SEP LC-52 system with a Diacel CHIRALPAK AS-H (particle size 5 μm, dimensions 250 mm × i.d. 4.6 mm).

Fungal material

Specimens of *Lentinula edodes* were acquired from Lijiang City, Yunnan Province, China, in 2016. Taxonomic identification was

established through molecular characterization of the ITS gene fragment. The resulting sequence (GenBank accession No. OQ680131) exhibited over 99% homology with reference sequences of *L. edodes* upon BLAST analysis, confirming its identity. A voucher specimen (No. HZYXG01) was deposited at the School of Pharmacy, Henan University of Chinese Medicine.

Extraction and isolation

The air-dried fruiting bodies of *L. edodes* (3.5 kg) were extracted with 95% EtOH (20 L × 4) at room temperature, each soaking lasting three days. The combined ethanolic extracts (80 L) were concentrated under reduced pressure to approximately 5 L and subsequently partitioned with EtOAc (5 L × 3). Evaporation of the EtOAc phase yielded 120 g of crude extract. This extract was subjected to flash silica gel column chromatography eluting with a petroleum ether-acetone gradient, affording seven fractions (A–G). Fraction E (24 g) was further separated by MPLC on a C-18 column using a gradient of CH_3OH–H_2O (from 20:80 to 100:0, V/V) to generate 14 subfractions (E1–E14).

Subfractions E4 (CH_3OH), E5 (acetone), and E6 (acetone) were further purified by size-exclusion chromatography on Sephadex LH-20. This process yielded 11 fractions (E4a–E4k) from E4, 9 fractions (E5a–E5i) from E5, and 12 fractions (E6a–E6l) from E6. Fraction E11 was divided on an MPLC equipped with an MCI column, eluted with CH_3OH–H_2O (V/V, from 20/80 to 0/100), yielding 12 subfractions (E11a–E11l). Compound **3** from E4k (3.5 mg, t_R = 7.2 min, CH_3CN/H_2O: 25/75 to 50/50, 25 min, flow rate 15 mL min^{-1}). Fraction E4a was subjected to Sephadex LH-20 (acetone), affording eight minor fractions (E4a1-E4a8), instead of four subfractions as previously.[10] Compound **4** (4.3 mg, t_R = 5.7 min) from fraction E4a8 was obtained by prep. HPLC (CH_3CN/H_2O: 60/40 to 85/15, 25 min, flow rate 15 mL min^{-1}). Compound **5** (1.9 mg, t_R = 11.4 min) from fraction E5e was purified by prep. HPLC (CH_3CN/H_2O: 15/85 to 30/70, 20 min, flow rate 7 mL min^{-1}). Compound **6** (2.8 mg, t_R = 14.6 min) from fraction E6c was purified by prep. HPLC (CH_3CN/H_2O: 15/85 to 35/65, 25 min, flow rate 7 mL min^{-1}). Compounds **1** (5.2 mg, t_R = 14.6 min) and **2** (5.0 mg, t_R = 16.1 min), both contained in fractions E6h to E6k, were purified by prep. HPLC (CH_3CN/H_2O: 15/85 to 35/65, 25 min, flow rate 7 mL min^{-1}).

Lentinuine A (3′*S*,6′*E*)-5-(6-ethoxy-5-hydroxy-2-methyl-4-oxochroman-2-yl)-2-methylpent-2-enoic acid (**1**): a yellow oil; $[\alpha]_D^{25}$ + 26.3 (*c* 0.023, CH_3OH), UV (MeOH) λ_{max} nm (log ε): 211 (4.33), 273 (3.86), 361 (3.51); IR (MeOH) ν_{max} cm^{-1}: 3452, 1683, 1607, 1490, 1251, 1075; ^{1}H NMR (600 MHz CD_3OD) and ^{13}C NMR (150 MHz CD_3OD) data see Table 1; HRESIMS *m*/*z* 357.1313 $[M + Na]^+$ (calcd 357.1309 for $C_{18}H_{22}O_6Na^+$).

(±) Lentinuine B (±) (6′*E*)-5-(8-hydroxy-2-methyl-4-oxochroman-2-yl)-2-methylpent-2-enoic acid (**2**): a yellow oil; UV (MeOH) λ_{max} nm (log ε): 213 (4.22), 266 (3.56), 340 (3.27); IR (MeOH) ν_{max} cm^{-1}: 3411, 1686, 1489, 1315, 1216, 1028; ^{1}H NMR (600 MHz CD_3OD) and ^{13}C NMR (150 MHz CD_3OD) data see Table 1. HRESIMS *m*/*z* 313.1044 $[M + Na]^+$ (calcd 313.1046 for $C_{16}H_{18}O_5Na^+$).

Single crystal X-ray diffraction data for **6**: $C_{13}H_{16}O_4$, M = 236.26, a = 4.86620(10) Å, b = 11.8867(3) Å, c = 10.8940(3) Å, α = 90°, β = 96.2720(10)°, γ = 90°, V = 626.37(3) $Å^3$, T = 100(2) K, space group $P2_1$, Z = 2, μ(CuKα) = 0.765 mm^{-1}, 6684 reflections measured, 2125 independent reflections (R_{int} = 0.0207). The final R_1 values were 0.0357 ($I > 2\sigma(I)$). The final w$R(F^2)$ values were 0.0979 ($I > 2\sigma(I)$). The final R_1 values were 0.0358 (all data). The final w$R(F^2)$ values were 0.0979 (all data). The goodness of fit on F^2 was 1.086. Flack parameter = 0.17(3). Crystallographic data have been deposited with the Cambridge Crystallographic Data Centre (deposition number CCDC 2474042).

Calculations of ECD and optical rotation

Conformational analysis of compound **1** was conducted using the MMFF94 s molecular mechanics force field. Conformers accounting for more than 1% of the Boltzmann distribution were subjected to further geometry optimization at the B3LYP/6-31G(d,p) level using Gaussian 16.[17] Optimized conformers within an energy window of 3 kcal mol^{-1} from the lowest-energy structure were then used for subsequent ECD and optical rotation calculations. Full computational details are provided in the SI.

ECD calculation. ECD calculations were carried out employing the TDDFT methodology as implemented in Gaussian 16.[17] Geometry optimization and subsequent ECD simulations were performed at the B3LYP/6-31G(d,p) level, incorporating solvent effects of methanol through the CPCM solvation model. The generated rotational strengths were converted into ECD curves using SpecDis version 1.70.1. The corresponding ECD spectra for the opposite enantiomers were produced by applying the "enantiomeric ECD" tool within the SpecDis software package.[18]

Optical rotation calculation. Optical rotation calculations were carried out using the Ground State method implemented in Gaussian 16 at the B3LYP/6-311+G(d,p) level of theory.[17] Solvent effects of methanol were set with the CPCM solvation model. The final specific rotation values for 3′*S*-**1** and *S*-**4** were obtained by Boltzmann-weighted averaging of conformer contributions using Microsoft Excel.

Biological assays

The DPPH free radical scavenging assay

Antioxidant activity was assessed using the DPPH radical scavenging assay adapted from a literature method.[19] Briefly, test compounds **1** and **2** were dissolved in ethanol to a final concentration of 50 μM and mixed with an equal volume of 100 μM DPPH solution. The reaction mixtures were kept in the dark at 30 °C for 60 min, after which the optical density at 515 nm was recorded. Trolox at 25 μM was employed as a reference antioxidant. For each experiment, control wells (containing DPPH solution without test compound) and blank wells (containing solvent only) were included. All measurements were conducted in triplicate. The percentage of DPPH radical inhibition was calculated according to the equation: inhibition (%) = $[1 - (OD_{sample} - OD_{blank})/(OD_{control} - OD_{blank})] \times 100$.

Evaluation of immunosuppressive activity, and antiproliferative effects on HaCaT cells

The immunosuppressive activity and antiproliferative activity against HaCaT cells were evaluated using the CCK-8 method in accordance with a previously described protocol.[10] In the immunosuppressive and lymphocyte viability assays, all compounds were initially tested at a concentration of 40.0 μM, with dexamethasone (2.0 μM) and mycophenolic acid (0.2 μM) utilized as positive controls. For the assessment of antiproliferative activity against HaCaT cells, compounds were screened at 40.0 μM, employing methotrexate (40.0 μM) as the positive control. Compounds exhibiting inhibition rates exceeding 50% in the primary screening were subsequently subjected to IC_{50} determination. All experiments were performed in triplicate.

Data processing and statistical analysis

Data processing and statistical analysis were carried out with GraphPad Prism 8.0. Values are reported as the arithmetic mean ± standard deviation ($\bar{x} \pm s$).

Ethic statement

The animal study (No. DWLL202003116) was reviewed and approved by the Animal Welfare Ethics Committee of Henan University of Chinese Medicine.

Molecular docking studies

Molecular structures of the enantiomers (*R*)-**2** and (*S*)-**2** were initially generated using ChemDraw 14.0 and subsequently converted to three-dimensional representations *via* Chem3D 14.0. For docking simulations, all water molecules were stripped from the receptor models, after which polar hydrogen atoms, Gasteiger charges, and magnetic field parameters were assigned using AutoDockTools version 1.5.6. Automated docking was performed with AutoDock Vina. The highest-scoring binding poses were identified and further analyzed; both two- and three-dimensional visualizations of these interaction modes were prepared using Discovery Studio Visualizer (release 20).

Author contributions

Zhen-Zhu Zhao: conceptualization, writing – review & editing, formal analysis, data curation, validation, supervision. Fei Zhang: writing – original draft, formal analysis, data curation. Qi-Lu Zhao: investigation. Jie Zhao: formal analysis, data curation. Hai-Rong He: writing – review & editing. Hai-Jiao Liu: investigation. Ke-Ke Liu: investigation. Hui Chen: writing – review & editing, supervision, funding acquisition, conceptualization.

Conflicts of interest

There are no conflicts to declare.

Data availability

CCDC 2474042 contains the supplementary crystallographic data for this paper.[20]

All data are available in the supplementary information (SI). Supplementary information: the 1D & 2D NMR, MS, calculation details, and crystallographic data of compounds **1–6**. See DOI: https://doi.org/10.1039/d5ra09796g.

Acknowledgements

This work was financially supported by the Natural Science Foundation of Henan (CN) (252300423171), the Science and Technology Innovative Research Team in Higher Educational Institutions of Henan Province (CN) (24IRTSTHN039), and the Scientific Research Nursery Project of Henan University of Chinese Medicine (CN) (MP2024-10).

Notes and references

1 E. Goyer, C. Lavaud and G. Massiot, *Nat. Prod. Rep.*, 2023, **40**(6), 1071–1077, DOI: 10.1039/d3np00004d.
2 M. Zhao, Y. Tang, J. Xie, Z. Zhao and H. Cui, *Eur. J. Med. Chem.*, 2021, **209**, 112860, DOI: 10.1016/j.ejmech.2020.112860.
3 R. Geris and T. J. Simpson, *Nat. Prod. Rep.*, 2009, **26**(8), 1063–1094, DOI: 10.1039/b820413f.
4 Z. Liang, T. Gu, J. Wang, J. She, Y. Ye, W. Cao, X. Luo, J. Xiao, Y. Liu, L. Tang and X. Zhou, *Bioorg. Chem.*, 2021, **112**, 104927, DOI: 10.1016/j.bioorg.2021.104927.
5 S. Gujarathi, M. K. Zafar, X. Liu, R. L. Eoff and G. Zheng, *Molecules*, 2020, **25**(24), 5847, DOI: 10.3390/molecules25245847.
6 X. Peng and M. Qiu, *Nat. Prod. Bioprospect.*, 2018, **8**(3), 137–149, DOI: 10.1007/s13659-018-0164-z.
7 S. Sakai, Y. Tomomura, H. Yoshida, S. Inoue and H. Kawagishi, *Biosci. Biotechnol. Biochem.*, 2005, **69**(8), 1630–1632, DOI: 10.1271/bbb.691630.
8 B. Baral, *Chem. Biodivers.*, 2025, **22**(12), e01244, DOI: 10.1002/cbdv.202501244.
9 Y. Yaoita, M. Kikuchi and K. Machida, *Nat. Prod. Commun.*, 2014, **9**(3), 419–426.
10 Z. Z. Zhao, F. Zhang, B. Y. Ji, N. Zhou, H. Chen, Y. J. Sun, W. S. Feng and X. K. Zheng, *RSC Adv.*, 2023, **13**(27), 18223–18228, DOI: 10.1039/d3ra02672h.
11 H. Koshino, T. Yoshihara, M. Okuno, S. Sakamura, A. Tajimi and T. Shimanuki, *Biosci. Biotechnol. Biochem.*, 1992, **56**(7), 1096–1699, DOI: 10.1271/bbb.56.1096.
12 J. Wu, T. Tokunaga, M. Kondo, K. Ishigami, S. Tokuyama, T. Suzuki, J. H. Choi, H. Hirai and H. Kawagishi, *J. Nat. Prod.*, 2015, **78**(1), 155–158, DOI: 10.1021/np500623s.
13 S. Sakai, Y. Tomomura, H. Yoshida, S. Inoue and H. Kawagishi, *Biosci. Biotechnol. Biochem.*, 2005, **69**(8), 1630–1632.
14 M. J. Burk, C. S. Kalberg and A. Pizzano, *J. Am. Chem. Soc.*, 1998, **120**, 4345–4353.

15 M. D. Sintchak, M. A. Fleming, O. Futer, S. A. Raybuck, S. P. Chambers, P. R. Caron and M. A. Murcko, *Cell*, 1996, **85**(6), 921–930.
16 E. M. Eugui, S. J. Almquist, C. D. Muller and A. C. Allison, *Scand. J. Immunol.*, 1991, **33**(2), 161–173, DOI: 10.1111/j.1365-3083.1991.tb03746.x.
17 M. J. Frisch, G. W. Trucks, H. B. Schlegel, G. E. Scuseria, M. A. Robb, J. R. Cheeseman, G. Scalmani, V. Barone, G. A. Petersson, H. Nakatsuji, X. Li, M. Caricato, A. V. Marenich, J. Bloino, B. G. Janesko, R. Gomperts, B. Mennucci, H. P. Hratchian, J. V. Ortiz, A. F. Izmaylov, J. L. Sonnenberg, D. Williams-Young, F. Ding, F. Lipparini, F. Egidi, J. Goings, B. Peng, A. Petrone, T. Henderson, D. Ranasinghe, V. G. Zakrzewski, J. Gao, N. Rega, G. Zheng, W. Liang, M. Hada, M. Ehara, K. Toyota, R. Fukuda, J. Hasegawa, M. Ishida, T. Nakajima, Y. Honda, O. Kitao, H. Nakai, T. Vreven, K. Throssell, J. A. Montgomery Jr., J. E. Peralta, F. Ogliaro, M. J. Bearpark, J. J. Heyd, E. N. Brothers, K. N. Kudin, V. N. Staroverov, T. A. Keith, R. Kobayashi, J. Normand, K. Raghavachari, A. P. Rendell, J. C. Burant, S. S. Iyengar, J. Tomasi, M. Cossi, J. M. Millam, M. Klene, C. Adamo, R. Cammi, J. W. Ochterski, R. L. Martin, K. Morokuma, O. Farkas, J. B. Foresman and D. J. Fox, *Gaussian 16, Revision B.01*,Gaussian, Inc., Wallingford CT, 2016.
18 T. Bruhn, A. Schaumloffel, Y. Hemberger and G. Pecitelli. *SpecDis version 1.71*, Berlin, Germany, 2017, https://specdis-software.jimdofree.com.
19 W. Jaidee, W. Maneerat, R. J. Andersen, B. O. Patrick, S. G. Pyne and S. Laphookhieo, *Fitoterapia*, 2018, **130**, 219–224, DOI: 10.1016/j.tote.2018.09.004.
20 CCDC 2474042: Experimental Crystal Structure Determination, 2025, DOI: 10.5517/ccdc.csd.cc2p1ft0.